

RESEARCH ARTICLE

Low-salinity water off West Luzon Island in summer

10.1002/2014JC010465

Yunwei Yan¹, Guihua Wang¹, Chunzai Wang², and Jilan Su¹

Key Points:

- Low-salinity water is found off West Luzon in summer
- Rainfall associated with the summer monsoon is responsible for its formation
- Low-salinity water has robust month-to-month and interannual variability

Correspondence to:

G. Wang,
wghocean@yahoo.com

Citation:

Yan, Y., G. Wang, C. Wang, and J. Su (2015), Low-salinity water off West Luzon Island in summer, *J. Geophys. Res. Oceans*, 120, 3011–3021, doi:10.1002/2014JC010465.

Received 21 SEP 2014

Accepted 17 MAR 2015

Accepted article online 23 MAR 2015

Published online 25 APR 2015

¹State Key Laboratory of Satellite Ocean Environment Dynamics, Second Institute of Oceanography, State Oceanic Administration, Hangzhou, China, ²NOAA/Atlantic Oceanographic and Meteorological Laboratory, Miami, Florida, USA

Abstract Low-salinity water with two cores is found off West Luzon Island in the South China Sea (SCS) during summer. A series of salinity observations and model results show that the low-salinity water begins to appear in June, reaches its lowest salinity in September, and disappears after October. Rainfall associated with the summer monsoon impinging on the Philippine mountain ranges plays an important role in the formation of the low-salinity water, while upward Ekman pumping of high-salinity subsurface water caused by the strong winter monsoon is important for its disappearance. Variation in mixed layer depth is responsible for the formation of the two cores of the low-salinity water, while advection also contributes. The study further demonstrates that the low-salinity water has considerable interannual variability associated with El Niño–Southern Oscillation (ENSO): during the summer of the decaying year of an El Niño, an anticyclonic wind anomaly occurs in the SCS. The anticyclonic wind anomaly is associated with a northeasterly anomaly south of 18°N, reducing precipitation and causing salting of the low-salinity water off West Luzon Island. The situation is reversed during the summer of the decaying year of a La Niña.

1. Introduction

Salinity is an important physical property of seawater. Like temperature, salinity also contributes to dynamic and thermodynamic variations in the ocean. Salinity partakes in the formation of water masses, thermohaline circulation, and climate processes. Evolution of salinity is controlled by several processes such as freshwater flux, horizontal advection, and water mass mixing. Compared with the ocean temperature, lack of ocean salinity measurement in the past has limited our understanding of the variability of the ocean salinity and its dynamics.

Salinity in the South China Sea (SCS) has been previously documented. Salinity was often used in water mass analysis to investigate the intrusion of the North Pacific water into the SCS [e.g., Xu and Su, 1997; Qu *et al.*, 2000; Yu *et al.*, 2008; Nan *et al.*, 2013]. Enhanced saline stratification induced by freshwater flux could limit wind-induced mixing in shallow mixed layers, leading to the formation of barrier layers [Pan *et al.*, 2006; Zeng *et al.*, 2009]. Salinity was also found to play a very important role in the bottom circulation of the SCS [Wang *et al.*, 2011].

Most of the studies mentioned above focused on basin-scale salinity variation. Only a few studies addressed variability of salinity in the SCS at the subbasin scale, partly due to the lack of observation. As shown in Figure 1a, heavy precipitation occurs off West Luzon Island in summer (referring to July, August, and September in this study) due to the southwest monsoon impinging on mountain ranges [Xu *et al.*, 2008]. Concurrently, Agno River, the third largest river in Luzon in terms of drainage area [Liu *et al.*, 2009], drains a large amount of freshwater into the area west of Luzon through Lingayen Gulf (summer and winter means at Carmen Station: 335 and 60 m³/s, respectively). A natural question is: is there significant salinity change in this part of the SCS due to the rainfall and runoff? If yes, what are the major processes for the salinity change? In this paper, through both observations and model results, we studied the summer mean climatology, month-to-month variation, and interannual variability of the salinity off West Luzon Island.

2. Data and Methods

2.1. Data

The Soil Moisture and Ocean Salinity (SMOS) satellite mission supported by European Space Agency (ESA) was launched in November 2009. It provides continuous sea surface salinity (SSS) data from 2010 on. In this

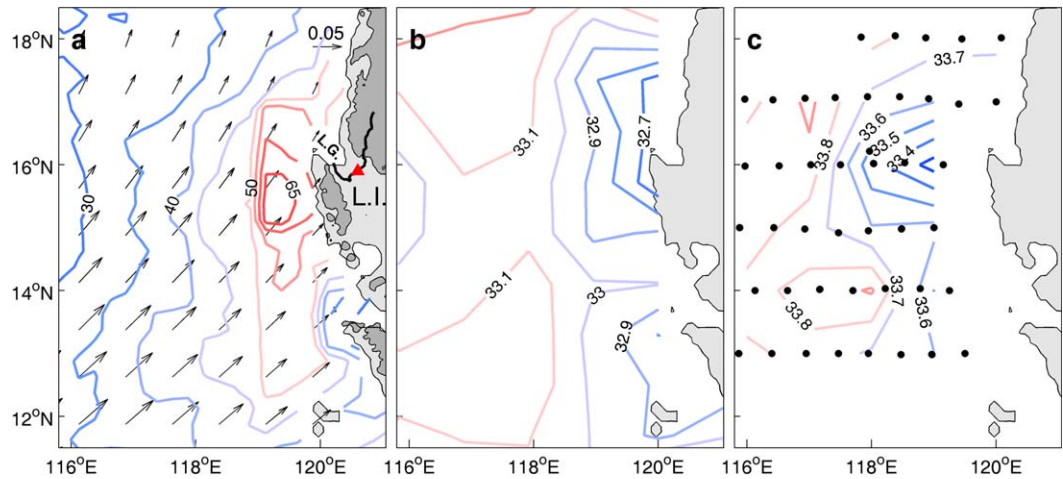


Figure 1. (a) The average summer TRMM precipitation (contours, cm/month) and CCMP wind stress vector (arrows, N/m^2), (b) the average summer SMOS sea surface salinity (SSS) (PSU) in 2010 and 2011, and (c) SSS observation (PSU) during the period from 1 to 18 July 1969 derived from the cruise SU000299 of World Ocean Database 2013. Black dots are observation stations. L.I. is Luzon Island. L.G. is Lingayen Gulf. Black line is Ango River, and red triangle is Carmen Station. Elevations greater than 300 m are shaded in gray.

study, SMOS SSS data are obtained from Production Center (CPDC) of the “Centre Aval de Traitement des Données SMOS” (CATDS). The reprocessed monthly salinity of level 3 product with a 100 km spatial resolution from 2010 to 2011 is used here. Recent work demonstrates that SMOS salinity data can capture the seasonal variability of SSS [Alory et al., 2012; Nyadjro et al., 2012].

Monthly multisatellite precipitation analysis (3B43V7) of Tropical Rainfall Measuring Mission (TRMM) [Huffman et al., 2007] from 1998 to 2011 is used to construct the precipitation climatology. The precipitation product, covering from 50°S to 50°N, merges four independent precipitation fields on a $0.25^\circ \times 0.25^\circ$ spatial resolution. Evaporation is derived from the ECWMF Interim Reanalysis (ERA-Interim), which is produced by the European Centre [Dee et al., 2011]. The data set has a horizontal resolution of $0.75^\circ \times 0.75^\circ$ from 1979 to 2011.

Wind stress climatology is obtained from Cross-Calibrated, Multi-Platform (CCMP) ocean surface wind product [Atlas et al., 2011], which combines a series of satellite and conventional observations extracted from ECMWF analysis using an enhanced variational analysis method. The product covers the global ocean with a 6 h time resolution and 25 km spatial resolution for the period beginning from 1987.

2.2. Mixed Layer Salinity Model

Following Price et al [1978], the salinity equation for the ocean mixed layer, ignoring horizontal advection, can be written as

$$\frac{\partial S}{\partial t} = \frac{(E-P)S}{h_m} - \frac{w_e \Delta S}{h_m} \tag{1}$$

where S is the mixed layer salinity (MLS); $E-P$ is evaporation minus precipitation; h_m is the mixed layer depth (MLD); w_e is the entrainment velocity with its positive direction upward; and ΔS is the salinity difference between the MLD and 30 m below the mixed layer base [Ren and Riser, 2009].

Different from Price et al. [1978], horizontal advection is considered in the estimate of the entrainment velocity w_e which, following Qu [2001], is calculated from equation (2).

$$\left. \begin{aligned} w_e &= \frac{\partial h_m}{\partial t} + w_{mb} + \mathbf{V} \cdot \nabla h_m, & \frac{\partial h_m}{\partial t} + w_{mb} + \mathbf{V} \cdot \nabla h_m &> 0 \\ w_e &= 0, & \frac{\partial h_m}{\partial t} + w_{mb} + \mathbf{V} \cdot \nabla h_m &< 0 \end{aligned} \right\} \tag{2}$$

where \mathbf{V} is the horizontal velocity and w_{mb} is the vertical velocity at the base of the mixed layer. Qu [2001] showed that w_{mb} is dominated by Ekman pumping in regions where the MLD is shallow.

The MLD is defined as the depth where the potential density (σ_θ) is equal to that at 10 m plus an increment in σ_θ equivalent to a net temperature decrease of 1.0°C [Qu, 2003; Mignot *et al.*, 2012]. We calculate the MLD using the diagnostic temperature/salinity profile from Generalized Digital Environment Model Version 3.0 data set (GDEM3) [Carnes, 2009].

2.3. Regional Ocean Modeling System (ROMS)

In this study, the ROMS [Shchepetkin and McWilliams, 2005], a three-dimensional ocean circulation model, is used to simulate salinity variation off West Luzon Island. The model covers the domain, (2°N–28°N) by (99°E–142°E), with a 1/12° horizontal resolution and 30 levels in the vertical direction. Details of the model configuration can be found in Wang *et al.* [2013].

To test the respective role of precipitation and runoff in the salinity distribution off West Luzon Island, we designed four model experiments as follows:

1. Control run—the model is integrated for 40 years with monthly climatological CCMP winds, ERA-Interim net heat flux, and freshwater flux including ERA-Interim evaporation, TRMM precipitation, and Agno River runoff. The salinity climatology is computed using the model outputs of the last 10 years.
2. Exp NoPR—the experiment is the same as the control run but without any freshwater input (i.e., both the precipitation and the Agno river discharge are set to zero).
3. Exp NoR—the experiment is the same as the control run but without the Agno River runoff.
4. Exp PYears—the model is forced by monthly forcing fields, but without Agno River runoff, from 1 January 1998 to 31 December 2011.

3. Results

3.1. Climatological Summer Mean Salinity Off West Luzon Island

Figure 1b shows the average satellite SSS in the summer of 2010 and 2011. The most conspicuous feature is the low-salinity water appearing in the area west of Luzon Island, extending from 118°E to 120°E in the zonal direction and from 13°N to 18°N in the meridional direction. The low-salinity water has two cores—the northern one is located near 16.5°N, while the southern one is located around 13.5°N, each surrounded by an SSS front. Their minimum salinity values inside the core are 32.7 PSU and 32.9 PSU, respectively. Salinity observation during the period from 1 July 1969 to 18 July 1969 derived from the cruise SU000299 of World Ocean Database 2013 (WOD13) shows a similar pattern (Figure 1c), indicating that in summer, the low-salinity water off West Luzon Island may be a common phenomenon.

ROMS is applied to the SCS to study the formation and structure of the low-salinity water. The model design is described in section 2.3. The simulated summer SSS of the control run exhibits a pattern of low-salinity water with two cores off West Luzon Island (Figure 2a), consistent with the observation. This suggests that the model can reproduce the low-salinity water very well. With no freshwater input from either precipitation or Agno River runoff (Exp NoPR), the low-salinity water disappears in the experiment (Figure 2b), suggesting that freshwater input plays an important role in the formation of the low-salinity water. If only precipitation is considered (Exp NoR), the low-salinity water off West Luzon is almost the same as that in the control run (Figure 2c), suggesting that precipitation is the principal factor for the formation of the low-salinity water off West Luzon Island.

To isolate the effect of precipitation on the low-salinity water, i.e., ignoring the effect of advection, we use monthly E-P to integrate the mixed layer salinity model from June to November. Because, in summer, evaporation (about 10 cm/month) is much less than precipitation (about 60 cm/month) off West Luzon Island (Figures 1a and 3a), the summer pattern of E-P is similar to that of precipitation (Figures 1a and 3b). With only the E-P term considered in equation (1), the water off West Luzon Island shows a low salinity distribution with two cores in summer (Figure 2d), which further verifies that precipitation is the principal factor for the formation of the low-salinity water. It is interesting to note that the low-salinity water has two cores, while the precipitation has only one core with a maximum value near 15.5°N (Figures 1a and 2d). The mismatch between the spatial patterns of salinity and precipitation, respectively, is likely caused by the variation in MLD.

In summer, the effect of MLD variation on SSS is mainly through the E-P term in equation (1) since w_e is basically zero during that time. The MLDs around the zonal band of 16.5°N and south of 13.0°N are relatively shallow (Figure 4a). Change in SSS due to E-P as computed from equation (1) shows two cores of the

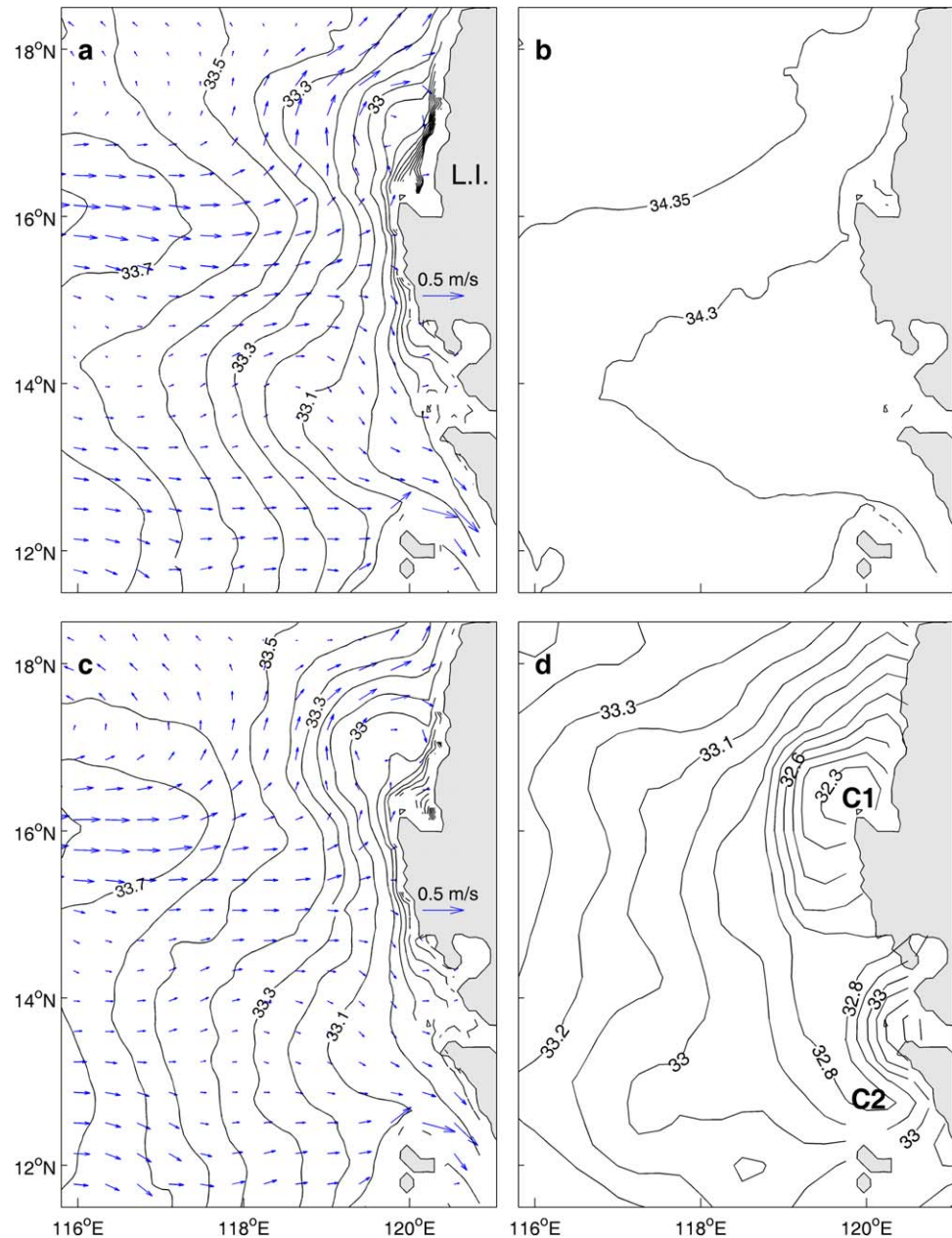


Figure 2. Summer mean climatology of SSS (PSU) from (a) the control run, (b) Exp NoPR, and (c) Exp NoR of the ROMS model, and from (d) the integration of mixed layer salinity model, equation (1), with only the monthly E-P. Blue vectors in Figures 2a and 2c are summer mean surface current. C1 and C2 in Figure 2d are two centers of low-salinity water.

low-salinity water (Figure 3c), suggesting that the MLD is important in the formation of the two cores. To further understand the spatial pattern of the MLD, we use equation (3) to compute the Monin-Obukhov depth (MOD), which is consistent with the MLD length scale [Caldeira and Marchesiello, 2002].

$$MOD = u_*^3 / (\kappa \times B_f) \tag{3}$$

where u_* is the friction velocity (proportional to the wind speed), B_f is the surface buoyancy flux (associated with both the heat flux and E-P), and κ is the von Karman's constant. Details about the MOD calculation can be found in Anitha et al. [2008]. The patterns of MOD and MLD are indeed similar and both show relatively shallow regions around 13.0°N and 16.5°N, respectively (Figures 4a and 4b). Not surprisingly, the spatial patterns of MOD and wind speed bear much resemblance (Figure 4b). Thus, wind speed is likely responsible for the spatial pattern of the MLD, including the two cores of the low-salinity water. In addition, the SSS

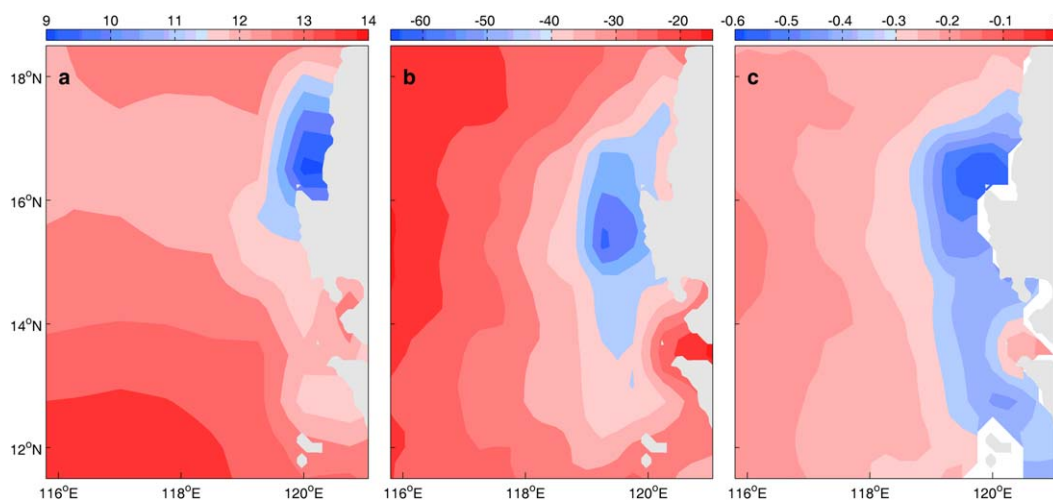


Figure 3. Summer mean of (a) evaporation (cm/month), (b) E-P (cm/month), and (c) SSS changes (PSU) induced by $\frac{(E-P)S}{h_m}$ derived from equation (1).

front surrounding the low-salinity water can also be seen from Figure 3c, suggesting that both the east to west decrease in precipitation and MLD distribution are important for the front.

Although the mixed layer model with only E-P forcing is capable of simulating the pattern of the low-salinity water, the salinity off West Luzon Island in the mixed layer model is generally lower than that in ROMS (Figures 2d and 2c). As advection is considered in ROMS but not in the mixed layer model, advection effect is likely to be the cause for the difference in salinity between the mixed layer model and ROMS. As shown in Figure 2c, ocean currents are mostly eastward off West Luzon Island in summer. These currents advect high-salinity water from the west to the east, increasing the salinity in the area west of Luzon. Note that the zonal currents along 15.5°N and 12.0°N are stronger than those along the other latitudes, thus bringing in more high-salinity water to the east and further strengthening the pattern of two low-salinity cores.

3.2. Monthly Variation of the Low-Salinity Water

Figure 5a shows monthly satellite SSS off West Luzon Island. The low-salinity water begins to appear in June, reaches its maximum area coverage in September, and disappears after October. High-quality salinity

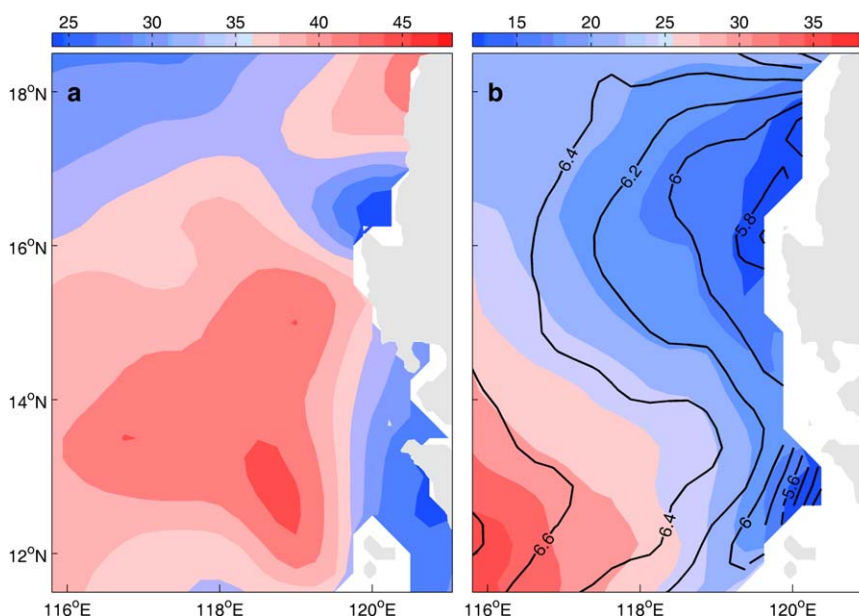


Figure 4. Summer mean of (a) mixed layer depth (m) and (b) Monin-Obukhov depth (color, m) and wind speed (contours, m/s).

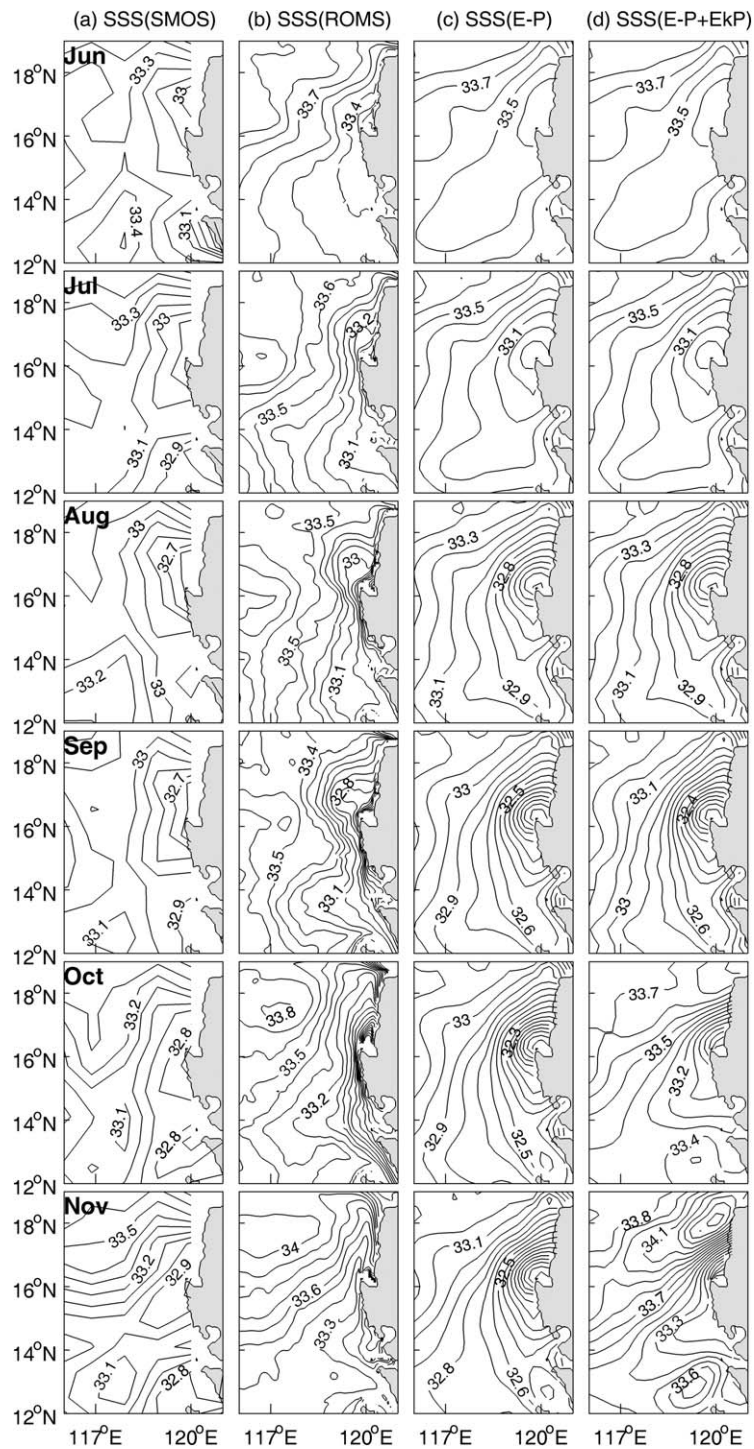


Figure 5. Month-to-month variation of salinity (a) derived from SMOS, (b) derived from ROMS, (c) calculated from equation (1) with only E-P term, and (d) calculated from equation (1) with E-P and Ekman pumping term. The interval is 0.1 PSU.

profiles provided by an Argo float (WMO 2901128) are also used to show the monthly salinity variation. Argo 2901128 was in the area of the low-salinity water from 1 June 2009 to 27 October 2009 (see insert map in Figure 6 for the track of the Argo float). The time interval of this Argo observation is 4 days. Monthly averaged salinity profiles are shown in Figure 6. Salinity profiles from this Argo float exhibit similar monthly variation: water in the mixed layer was much fresher in July to September than June, and became saltier again after September.

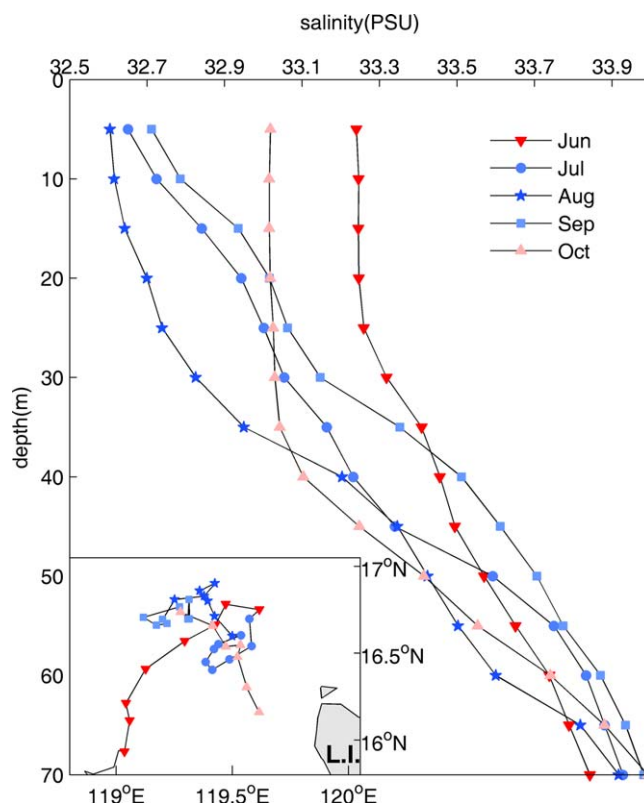


Figure 6. Monthly salinity profiles of Argo with platform number 2901128. The inserted map at the bottom left shows the trajectory of Argo 2901128. Profiles in rectangle (119.00°E–119.75°E, 16.25°N–17.00°N) are linearly interpolated into 14 vertical levels from 5 to 70 m with 5 m interval. Then, the monthly mean values are obtained with the interpolated profiles.

Monthly SSS climatology off West Luzon Island derived from ROMS also shows similar variation (Figure 5b). The low-salinity water is freshened gradually from June, attains its lowest salinity in September, and becomes saltier again after October. There is a slight difference between the ROMS and satellite data on the month when the lowest salinity occurs off West Luzon Island. The lowest salinity is in September for the ROMS data but in August/September for satellite data, probably because the ROMS data are climatological while the satellite data are only for the years 2010 and 2011.

In section 3.1, we have shown the importance of precipitation for the formation of the low-salinity water off West Luzon Island in summer. It is useful to examine the role of precipitation in the monthly variation of the low-salinity water. Strong precipitation associated with the orographic effects of the Philippine mountain ranges on summer monsoon [Xu *et al.*, 2008] appears in June, intensifies gradually in July and August, and then weakens in September when the monsoon reverses from southwesterly to north-

easterly (Figure 7a). As evaporation is much less than precipitation off West Luzon Island (Figures 7a and 7b), the monthly variation of E-P is in general similar to that of precipitation (Figure 7c).

When only E-P is considered, the mixed layer model shows that the low-salinity water is gradually freshened from June to September (Figure 5c), consistent with both ROMS and observations. This suggests that precipitation is important in the monthly variation of the low-salinity water. However, the highest precipitation occurs in August while the lowest salinity happens in September. The reason is that in September, precipitation is still greater than evaporation, causing a continuing decrease of salinity off West Luzon Island. From October to November, the simulated salinity in the mixed layer model remains low but the low-salinity water in ROMS quickly disappears after September, especially in the area northwest of Luzon. This suggests that other processes are responsible for the disappearance of the low-salinity water.

In fact, when the monsoon reverses from southwesterly to northeasterly after September, besides the cessation of the strong rainfall off West Luzon Island, the Ekman pumping is also reversed (Figure 7d). The Ekman pumping off West Luzon Island is downward from June to September but turns upward in October and November [Shaw *et al.*, 1996]. The upward Ekman pumping induced by the northeast monsoon [Wang *et al.*, 2008b] can bring high-salinity subsurface water into the mixed layer. When both E-P and Ekman pumping are considered in the mixed layer model, salting of the low-salinity water off West Luzon Island is well produced in October and November (Figure 5d). The pattern is consistent with both the observations and ROMS (Figures 5a and 5b). This suggests that the upward Ekman pumping induced by the northeast monsoon plays an important role in the disappearance of the low-salinity water.

3.3. Interannual Variability of the Low-Salinity Water

Figure 8 shows salinity observations during the summer of 1998 and 2000. Both show the low-salinity water off West Luzon Island, but the summer salinity in 1998 is much higher than that in 2000. The average

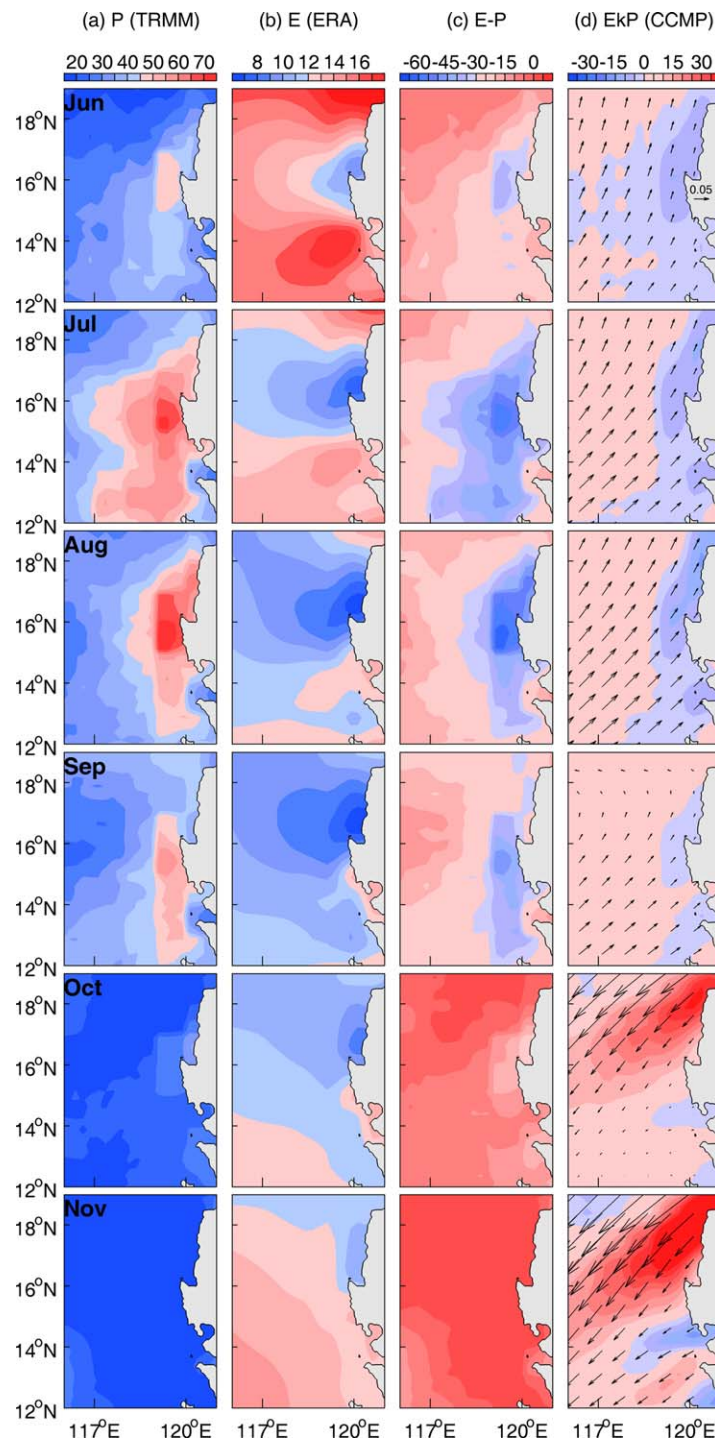


Figure 7. Month-to-month variation of (a) precipitation (cm/month), (b) evaporation (cm/month), (c) E-P (cm/month), and (d) wind stress vector (arrows) and Ekman pumping velocity (color, m/month).

southwesterly winds results in a reduced precipitation associated with the orographic effects of the Philippine mountain ranges (Figure 9a). Thus, the low-salinity water off West Luzon Island during the decay year of an El Niño has the minimum salinity higher than average (Figure 9b). The reverse is true during the decay year of a La Niña.

surface salinity in the area (118°E–120°E, 13°E–18°E) in the years 1998 and 2000 are 33.9 PSU and 33.0 PSU, respectively, suggesting that the low-salinity water may have considerable interannual variability. We note that 1998 is the decay year of an El Niño and 2000 is the decay year of a La Niña. This brings in the question whether the interannual variability of the low-salinity water is associated with El Niño–Southern Oscillation (ENSO).

To investigate the interannual variability of the low-salinity water off West Luzon Island, multivariate empirical orthogonal function (MV-EOF) analysis of zonal and meridional winds, precipitation, and SSS from the model experiment Exp PYears is conducted for the summers of the period 1998–2011. Figure 9 shows the spatial patterns and the principal component (PC) for the leading mode of the MV-EOF. The leading mode accounts for 64.8% of the total variance. The PC time series shows considerable interannual variability associated with ENSO, as evidenced by the high correlation coefficient (0.81) between the PC and January Niño3.4 SST indices (Figure 9c). The interannual time scale relationship between precipitation and the low-salinity water can be explained as follows: during the summer of the decay year of an El Niño, an anticyclonic wind anomaly occurs in the SCS [Wang et al., 1999], which yields a northeasterly anomaly south of 18°N [Wang et al., 2000, 2008a]. The weakened

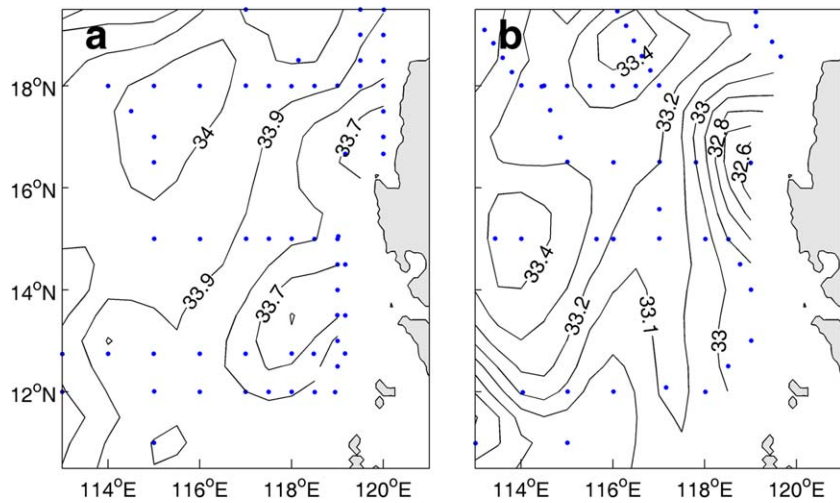


Figure 8. Spatial pattern of salinity (a) during 21–29 June 1998 derived from South China Sea Monsoon Experiment and (b) during 29 July 2000 to 7 August 2000. Blue dots are CTD stations.

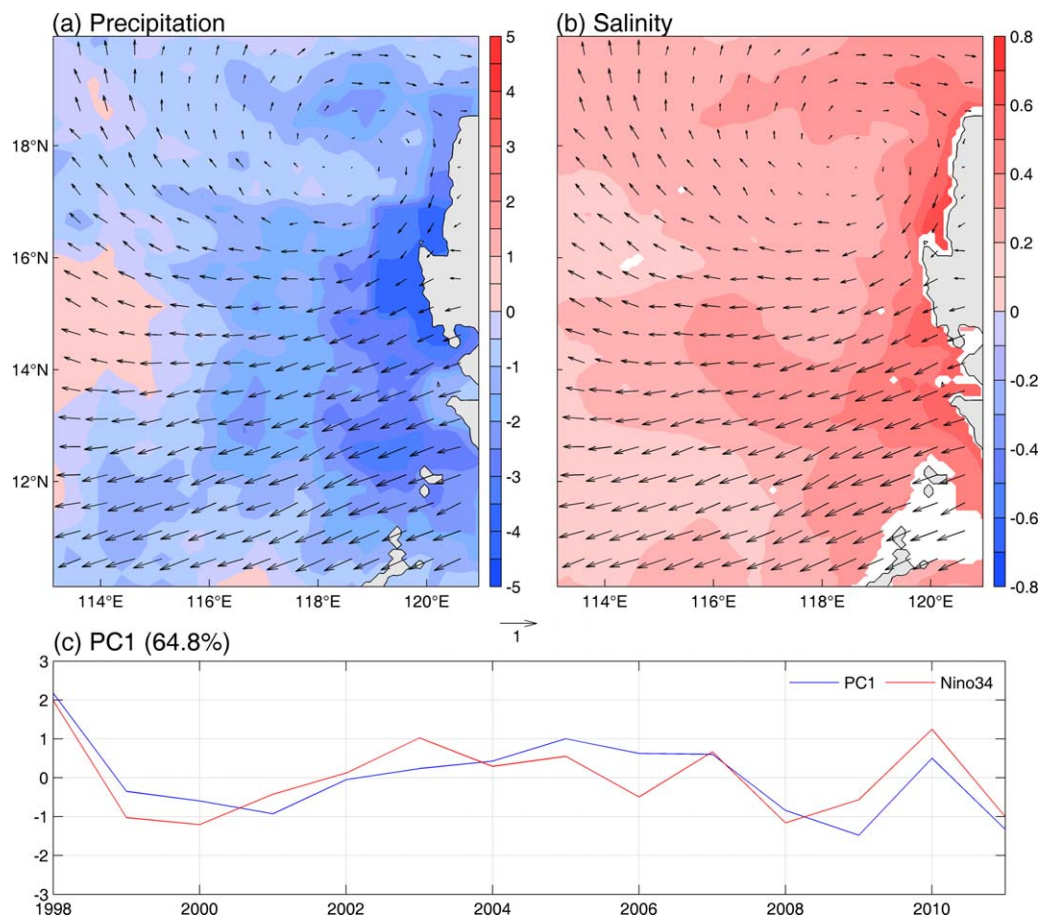


Figure 9. Spatial patterns (in color) of the anomalous (a) precipitation (mm/d) and (b) salinity (PSU), and (c) the corresponding principal component for the first MV-EOF mode (PC1). In Figures 9a and 9b, the anomalous summer wind vectors (m/s) are also plotted. In Figure 9c, the correlation coefficient between PC1 (blue) and January Nino3.4 SST (red) is 0.81 that is significant at the 95% level based on a *t* test.

4. Summary and Discussion

Using recently available salinity data, low-salinity water with two cores is found off West Luzon Island in summer. Our results show that precipitation induced by orographic effects is responsible for the formation of the low-salinity water. The two cores of the low-salinity water are mainly determined by both precipitation and MLD and enhanced by advection.

The low-salinity water begins to appear in June, reaches its lowest salinity in September and gradually disappears in October and November. Upward Ekman pumping of subsurface high-salinity water due to the northeasterly monsoon is important for the disappearance of the low-salinity water.

The low-salinity water also shows remarkable interannual variability associated with ENSO: Under the influence of El Niño (La Niña), an anticyclonic (a cyclonic) wind anomaly occurs in the SCS in the following summer, reducing (increasing) precipitation off West Luzon Island and further causing salting (freshening) of the low-salinity water.

Although multitime scale variability and formation mechanisms of the low-salinity water have been identified in this study, intraseasonal and shorter time scale variability of the low-salinity water needs to be further studied.

Acknowledgments

SMOS SSS data are obtained from Production Center of the "Centre Aval de Traitement des Données SMOS," operated for the "Centre National d'Etudes Spatiales" by IFREMER (<http://www.catds.fr/Products/Available-products-from-CPDC>). TRMM precipitation data are provided by the Goddard Distributed Active Archive Center (http://trmm.gsfc.nasa.gov/data_dir/data.html). CCMP wind data are derived from the Physical Oceanography Distributed Active Archive Center at the NASA Jet Propulsion Laboratory (<http://podaac.jpl.nasa.gov>). This study was supported by the National Science Foundation of China (NSFC) for Distinguished Young Scholars (41125019), the Major Research plan of the National Natural Science Foundation of China (91428206), the National Basic Research Program of China (2013CB430301), the NSFC (41321004 and 41306024), Basic Research Program of Second Institute of Oceanography, State Oceanic Administration (JT1301), and the base funding of NOAA/AOML. The authors wish to express their appreciation to the comments and suggestions of the Editor and the three anonymous reviewers.

References

- Alory, G., C. Maes, T. Delcroix, N. Reul, and S. Illig (2012), Seasonal dynamics of sea surface salinity off Panama: The far Eastern Pacific Fresh Pool, *J. Geophys. Res.*, *117*, C04028, doi:10.1029/2011JC007802.
- Anitha, G., M. Ravichandran, and R. Sayanna (2008), Surface buoyancy flux in Bay of Bengal and Arabian Sea, *Ann. Geophys.*, *26*(3), 395–400.
- Atlas, R., R. N. Hoffman, J. Ardizzone, S. M. Leidner, J. C. Jusem, D. K. Smith, and D. Gombos (2011), A cross-calibrated, multiplatform ocean surface wind velocity product for meteorological and oceanographic applications, *Bull. Am. Meteorol. Soc.*, *92*, 157–174, doi:10.1175/2010BAMS2946.1.
- Caldeira, R., and P. Marchesiello (2002), Ocean response to wind sheltering in the Southern California Bight, *Geophys. Res. Lett.*, *29*(13), 1635, doi:10.1029/2001GL014563.
- Carnes, M. R. (2009), Description and evaluation of GDEM-V3.0, *NRL Rep. NRL/MR/7330-09-9165*, Nav. Res. Lab., Washington, D. C.
- Dee, D. P., et al. (2011), The ERA-Interim reanalysis: Configuration and performance of the data assimilation system, *Q. J. R. Meteorol. Soc.*, *137*, 553–597.
- Huffman, G. J., R. F. Adler, D. T. Bolvin, G. Gu, E. J. Nelkin, K. P. Bowman, Y. Hong, E. F. Stocker, and D. B. Wolff (2007), The TRMM multi-satellite precipitation analysis: Quasi-global, multi-year, combined-sensor precipitation estimates at fine scale, *J. Hydrometeorol.*, *8*(1), 38–55.
- Liu, Z., Y. Zhao, C. Colin, F. P. Siringan, and Q. Wu (2009), Chemical weathering in Luzon, Philippines from clay mineralogy and major-element geochemistry of river sediments, *Appl. Geochem.*, *24*(11), 2195–2205.
- Mignot, J., A. Lazar, and M. Lacarra (2012), On the formation of barrier layers and associated vertical temperature inversions: A focus on the northwestern tropical Atlantic, *J. Geophys. Res.*, *117*, C02010, doi:10.1029/2011JC007435.
- Nan, F., H. Xue, F. Chai, D. Wang, F. Yu, M. Shi, P. Guo, and P. Xiu (2013), Weakening of the Kuroshio Intrusion into the South China Sea over the Past Two Decades, *J. Clim.*, *26*, 8097–8110.
- Nyadjro, E. S., B. Subrahmanyam, V. S. N. Murty, and J. F. Shriver (2012), The role of salinity on the dynamics of the Arabian Sea mini warm pool, *J. Geophys. Res.*, *117*, C09002, doi:10.1029/2012JC007978.
- Pan, A., X. Wan, J. Xu, X. Guo, and L. Li (2006), Characteristics and formation mechanisms of barrier layer in the northern east of South China Sea [in Chinese], *Chin. Sci. Bull.*, *51*(8), 951–957.
- Price, J. F., C. N. K. Mooers, and J. C. Van Leer (1978), Observation and simulation of storm-induced mixed-layer deepening, *J. Phys. Oceanogr.*, *8*, 582–599.
- Qu, T. (2001), Role of ocean dynamics in determining the mean seasonal cycle of the South China Sea surface temperature, *J. Geophys. Res.*, *106*(C4), 6943–6955, doi:10.1029/2000JC000479.
- Qu, T. (2003), Mixed layer heat balance in the western North Pacific, *J. Geophys. Res.*, *108*(C7), 3242, doi:10.1029/2002JC001536.
- Qu, T., H. Mitsudera, and T. Yamagata (2000), Intrusion of the North Pacific waters into the South China Sea, *J. Geophys. Res.*, *105*(C3), 6415–6424, doi:10.1029/1999JC900323.
- Ren, L., and S. C. Riser (2009), Seasonal salt budget in the northeast Pacific Ocean, *J. Geophys. Res.*, *114*, C12004, doi:10.1029/2009JC005307.
- Shaw, P.-T., S.-Y. Chao, K.-K. Liu, S.-C. Pai, and C.-T. Liu (1996), Winter upwelling off Luzon in the northeastern South China Sea, *J. Geophys. Res.*, *101*(C7), 16,435–16,448, doi:10.1029/96JC01064.
- Shchepetkin, A. F., and J. C. McWilliams (2005), The Regional Oceanic Modeling System (ROMS): A split-explicit, free-surface, topography-following-coordinate oceanic model, *Ocean Modell.*, *9*, 347–404.
- Wang, B., R. Wu, and X. Fu (2000), Pacific-East Asian teleconnection: How does ENSO affect East Asian climate?, *J. Clim.*, *13*, 1517–1536.
- Wang, B., Z. Wu, J. Li, C.-P. Chang, Y. Ding, and G. Wu (2008a), How to measure the strength of the East Asian summer monsoon?, *J. Clim.*, *21*, 4449–4463.
- Wang, C., R. H. Weisberg, and J. Virmani (1999), Western Pacific interannual variability associated with the El Niño-Southern Oscillation, *J. Geophys. Res.*, *104*(C3), 5131–5149.
- Wang, G., D. Chen, and J. Su (2008b), Winter eddy genesis in the eastern South China Sea due to orographic wind jets, *J. Phys. Oceanogr.*, *38*, 726–732, doi:10.1175/2007JPO3868.1.
- Wang, G., S.-P. Xie, T. Qu, and R. X. Huang (2011), Deep South China Sea circulation, *Geophys. Res. Lett.*, *38*, L05601, doi:10.1029/2010GL046626.
- Wang, G., L. Ling, R. Wu, and C. Chen (2013), Impacts of the Madden-Julian oscillation on the summer South China Sea ocean circulation and temperature, *J. Clim.*, *26*, 8084–8096.

- Xu, H., S.-P. Xie, Y. Wang, W. Zhuang, and D. Wang (2008), Orographic effects on South China Sea summer climate, *Meteorol. Atmos. Phys.*, *100*, 275–289, doi:10.1007/s00703-008-0309-4.
- Xu, J., and J. Su (1997), Hydrographic analysis on the intrusion of the Kuroshio into the South China Sea: II. Observational results during the cruise from August to September in 1994[J] [in Chinese], *Trop. Oceanol.*, *16*(2), 1–23.
- Yu, Z., J. P. McCreary, M. Yaremchuk, and R. Furue (2008), Subsurface salinity balance in the South China Sea, *J. Phys. Oceanogr.*, *38*, 527–539, doi:10.1175/2007JPO3661.1.
- Zeng, L., Y. Du, S.-P. Xie, and D. Wang (2009), Barrier layer in the South China Sea during summer 2000, *Dyn. Atmos. Oceans*, *47*(1-3), 38–54, doi:10.1016/j.dynatmoce.2008.08.001.